doi:10.26443/seismica.v2i4.1177

Inner forearc faults in northern Cascadia do not accommodate elastic strain driven by the megathrust seismic cycle

Nicolas Harrichhausen * [1, 2], **Kristin D Morell** [2], **Christine Regalla** [3]

[1]Univ. Grenoble Alpes, Univ. Savoie Mont Blanc, CNRS, IRD, Univ. Gustave Eiffel, ISTerre, Grenoble, France, [2]Department of Earth Science, University of California, Santa Barbara CA, USA, [3]School of Earth and Sustainability, Northern Arizona University, Flagstaff AZ, USA

Author contributions: *Conceptualization*: N. Harrichhausen, K.D. Morell, C. Regalla. *Methodology*: N. Harrichhausen. *Formal Analysis*: N. Harrichhausen. *Writing - Original draft*: N. Harrichhausen. *Writing - Review & Editing*: N. Harrichhausen, K.D. Morell, C. Regalla. *Visualization*: N. Harrichhausen. *Supervision*: K.D. Morell, C. Regalla. *Project administration*: K.D. Morell, C. Regalla. *Funding acquisition*: N. Harrichhausen, K.D. Morell, C. Regalla.

Abstract We employ numerical models to explore the connection between subduction zone coupling or megathrust rupture and upper plate faults in the northern Cascadia forearc. Active forearc faults north of the Olympic Peninsula exhibit similar characteristics: west-northwest strike, oblique right-lateral slip senses, and low slip rates (<1 mm/yr), but a potential to generate large (M ∼ 7) earthquakes. Previous hypotheses suggest stress in the upper plate from interseismic coupling or coseismic rupture on the subduction zone interface could drive permanent forearc strain. To test these hypotheses, we used a 3D boundary element method model to predict slip on the Leech River–Devils Mountain fault system if interseismic coupling or coeseismic rupture cause deformation. Our model predicts reverse left-lateral slip if strain results solely from subduction zone coupling, or normal right-lateral slip if the faults accommodate strain from a megathrust rupture. These results contradict observed fault kinematics. By modelling strain partitioning, where only the strain from the strike-slip component of subduction zone coupling is accommodated in the forearc, we also predict slip that is inconsistent with observed fault kinematics. These models challenge the hypothesis that subduction interface coupling or coseismic rupture are the primary driver of permanent forearc deformation in northern Cascadia.

Production Editor:
Alice-Agnes Gabriel
Christie Rowe
Handling Editor:
Harold Tobin
Copy & Layout Editor:
Théa Ragon

Received:
January 15, 2024
Accepted:
May 31, 2024
Published:
July 2, 2024

1 Introduction

At subduction zones, partial to full coupling of the down-going oceanic slab against the upper plate results in strain in the upper plate crust. Some of this strain is released as elastic rebound during megathrust earthquakes (e.g., Dragert et al., 1994; Leonard et al., 2004), while some may remain as permanent strain resulting in faulting and folding in the upper plate (e.g., Bellier et al., 1997; Marshall et al., 2000; Sieh and Natawidjaja, 2000). This faulting in the upper plate can be a significant source of seismic hazard (e.g., Johnson et al., 1999; Quigley et al., 2012; Ryder et al., 2012; Mouslopoulou et al., 2015), and constraining how strain is partitioned into permanent and elastic components is important in understanding this hazard. Additionally, quantifying permanent deformation in the upper crust can also provide information on what controls subduction zone coupling, such as plate roughness and topography, age of the oceanic plate, curvature of the margin, and the obliquity of convergence (e.g., Sitchler et al., 2007; Allmendinger and González, 2010; Morell et al., 2013).

Despite the importance of understanding permanent forearc deformation, the processes driving this strain are not completely understood. At several subduction zones, permanent deformation of the upper plate crust is thought to be driven by interseismic coupling on the subduction zone interface (e.g., McCaffrey et al., 2000; Wallace et al., 2004; Loveless et al., 2010; Feng et al., 2012; Delano et al., 2017). Some models argue that strain resulting from oblique coupling on the megathrust is partitioned spatially, with strike-slip faulting accommodating margin-parallel strain in the onshore inner forearc, and reverse faulting and folding accommodating margin-perpendicular strain occurring in the offshore outer forearc (e.g., Kimura, 1986; McCaffrey, 1991; Wang et al., 2007). However, other stresses are also thought to contribute to permanent strain. Some models argue that forearc faulting could also be induced by stress changes related to coseismic rupture during large megathrust earthquakes (Loveless et al., 2010; Duckworth et al., 2021). Additionally, several subduction zones have inner forearc maximum horizontal stress (S_{Hmax}) orientations derived from crustal seismicity that are perpendicular to plate convergence at the margin, contrary to convergence-parallel S_{Hmax} orientations that interseismic coupling is expected to induce (e.g., Wang, 2000; Townend and Zoback, 2006; Balfour et al., 2011; Townend et al., 2012; Dimitrova et al., 2016). These results suggest permanent forearc strain is not controlled solely by subduction zone coupling or coseismic rupture of the megathrust, and instead may reflect the background stress state of the forearc and arc.

*Corresponding author: n.harrichhausen@univ-grenoble-alpes.fr

Our models test if the stress induced by either interseismic subduction zone coupling or coseismic megathrust rupture can explain the observed kinematics and slip history of Holocene-active forearc faults. We use a 3D Boundary Element Method (BEM) model to predict fault kinematics of the Leech River–Devils Mountain fault system (LRDM) in northern Cascadia if they result solely from stress induced by geodetically-derived interseismic coupling on the subduction zone megathrust, or conversely, stress resulting from coseismic slip on the megathrust (e.g., Delano et al., 2017; Duckworth et al., 2021). This fault system is unique in that it transects the entire $\sim$ 20 to 25 km wide onshore forearc in northern Cascadia, allowing us to examine margin-perpendicular variations in forearc strain. We analyze the effects of strain partitioning by seperately considering the effects of only the strike-slip component of subduction zone coupling versus unpartitioned coupling. We then compare these results to previous paleoseismic studies and instrumental seismicity along this fault system to determine if interseismic strain, partitioned interseismic strain, or coseismic strain alone can explain the observed fault kinematics. These analyses test the degree to which active forearc faults relieve the stress imposed by the megathrust throughout its seismic cycle.

2 Tectonic Setting

At the Cascadia subduction zone, the Juan de Fuca (JdF) plate subducts towards the northeast beneath the North America (NA) plate at a rate of $\sim$ 40 mm /yr (Fig. 1; Yoshioka et al., 2005). Relative plate motion, subduction zone geometry, and subduction obliquity vary substantially along strike from south to north along the margin. At the southern extent of the subduction zone, the trench is oriented $\sim$ N–S, and JdF-NA plate motion is highly oblique, with an $\sim$2:1 ratio between slab-strike perpendicular and slab-strike parallel (right-lateral) components of relative plate motion (e.g., DeMets et al., 2010; Finley et al., 2019). In northern Cascadia, the trench is oriented $\sim$ NW–SE and JdF-NA plate motion is near-orthogonal, with a $\sim$ 4 : 1 ratio between the slab-strike perpendicular and left-lateral slab-parallel components (Fig. 1; e.g., DeMets et al., 2010; Finley et al., 2019).

Global navigation system satellite (GNSS) surface velocities of the forearc relative to the stable portion of the NA plate reflect this change in obliquity and the broader tectonics of the region (Fig. 1). At the southernmost extent of Cascadia (Mendocino triple junction), surface velocities are directed towards the northwest, partially as a result of northwest motion of the Sierra Nevada–Great Valley block and westward motion of the Basin and Range (Wells et al., 1998; McCaffrey et al., 2000; Wells and McCaffrey, 2013; McKenzie and Furlong, 2021). GNSS velocities gradually rotate clockwise further north until they are approximately parallel with JdF–NA relative plate motion in northern Oregon (Fig. 1). In northern Cascadia, at the northern limit of the JdF plate and the subduction zone, northeastward directed velocities are significantly diminished (Fig. 1)

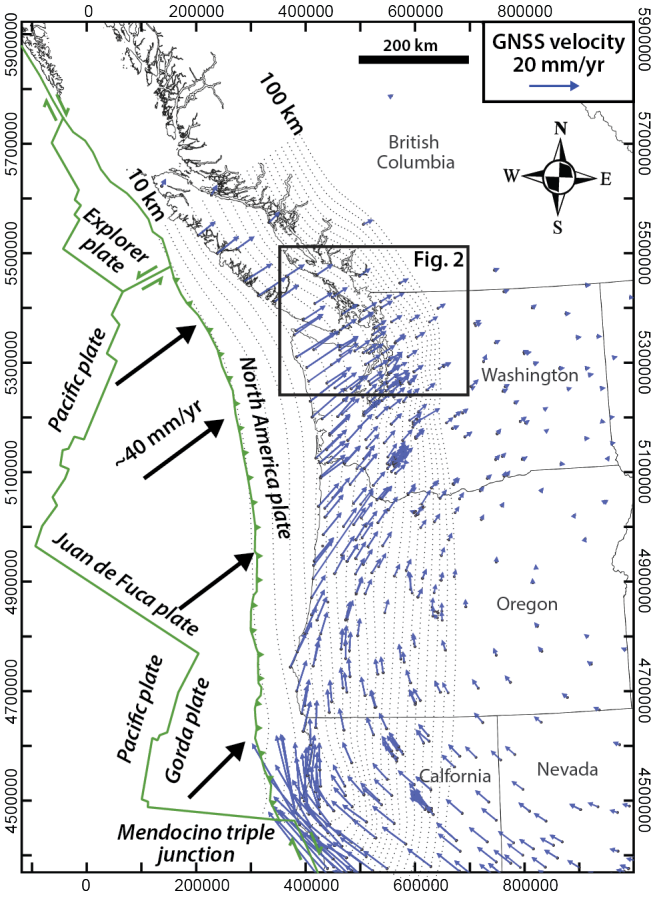

Figure 1 Tectonic setting of northern Cascadia with selected GNSS velocity vectors (thin blue arrows) showing motion with respect to stable North America (UNAVCO, McCaffrey et al., 2013). Juan de Fuca plate motion with respect to North America (DeMets et al., 2010) shown in thick black arrows. Juan de Fuca slab depth contours (Blair et al., 2011) are shown with dotted lines and are 10 km intervals. UTM grid coordinates (m) are in NAD83 UTM Zone 10N.

reflecting a cessation of subduction at the boundary between the JdF and Explorer plates (Savard et al., 2020).

The GNSS velocities (Fig. 1) show that the Cascadia subduction zone experiences partial to full interseismic coupling along the megathrust for the entire length of the subduction zone (Dragert et al., 1994; Hyndman and Wang, 1995; Wang et al., 2003; Schmalzle et al., 2014; Li et al., 2018b). Subduction zone coupling occurs offshore of western North America, a region we term the 'outer forearc', while onshore beneath the 'inner forearc', there is little to no measurable coupling from GNSS data (Schmalzle et al., 2014; Li et al., 2018b). The latest geodetic models suggest that the width of megathrust coupling in map view varies from $\sim$ 50 km in southern Cascadia, to $\sim$ 100 km near the Olympic Mountains, to $\sim$ 60 km in northern Cascadia near Vancouver Island (e.g., Li et al., 2018b) , although these coupling estimations contain substantial uncertainty due to insufficient seafloor geodetic data (Wang et al., 2003; Wang and Tréhu, 2016). The wider zone of coupling beneath the Olympic Mountains is due to a lesser slab dip where there is a bend in the subducting JdF Plate (Fig. 1; Li et al., 2018b). Slab dip partially controls the width of the

coupled zone because the downdip extent of coupling in warm subduction zones, such as Cascadia, is thought to be thermally controlled by the brittle-ductile transition (e.g., Hyndman and Wang, 1993; Hyndman et al., 1997; Oleskevich et al., 1999). The up-dip extent of coupling may also be thermally controlled, in this instance by the depth at which clay-dehydration reactions occur (e.g., Vrolijk, 1990; Hyndman and Wang, 1995; Moore and Saffer, 2001). In addition to the width of the coupled zone varying along strike, the degree to which the plates are coupled to each other varies along-strike within the coupled zone (Schmalzle et al., 2014; Li et al., 2018b).

Partial coupling in northern Cascadia is characterized by persistent subduction zone creep, and episodic tremor and slip (ETS) that recover a portion of the elastic deformation of the upper crust (McCaffrey, 2009; Schmalzle et al., 2014). ETS may be influenced by in-situ dehydration reactions of oceanic crust (Fagereng et al., 2018; Condit et al., 2020), with increased pore-fluid pressure resulting in tremor. Along-strike changes in sediment thickness on the downgoing slab, and lithology and porosity of the upper plate, can affect pore fluid generation and pressure; therefore controlling ETS, persistent creep, and the degree of coupling (e.g., Audet and Bürgmann, 2014; Schmalzle et al., 2014; Wells et al., 2017; Savard et al., 2018). Along-strike changes in upper plate roughness also affect the degree of coupling along the subduction interface (e.g. Wang and Bilek, 2014; Bassett and Watts, 2015; Van Rijsingen et al., 2019). These changes in subduction zone properties along-strike have resulted in spatially variable coupling that is dependant not only on slab dip.

The presence and spatial variability of coupling along the Cascadia subduction interface drives elastic deformation such as coastal uplift measured from tide gauges (Burgette et al., 2009), and to some degree, permanent deformation such as long-term uplift on the Olympic Peninsula deduced from river terraces (Delano et al., 2017). Far-field tectonic stresses, such as those related to Basin and Range extension (in southern Cascadia) and distributed right-lateral shear between the Pacific and NA plates (e.g., Pezzopane and Weldon, 1993; Wells et al., 1998; McCaffrey et al., 2000, 2007; Wells and McCaffrey, 2013; McKenzie and Furlong, 2021; Littel et al., 2023), and stress related to margin parallel mantle convection (e.g., Sternai et al., 2014; Chen et al., 2016) may also play a role in driving permanent strain that is observed in the upper plate. This permanent forearc deformation is recorded in Cascadia by oroclinal bending, rock uplift, active crustal faulting, and instrumental seismicity (Fig. 2; e.g., McCaffrey, 1992; Loveless et al., 2010; Delano et al., 2017; Malatesta et al., 2018; Finley et al., 2019; Harrichhausen et al., 2023).

In the inner forearc of northern Cascadia, north of the Olympic Mountains, several active faults accommodating permanent strain have been identified through paleoseismic observations and instrumental seismicity. These faults form a network of subvertical to steeply N-dipping W- to NW-striking structures that have hosted Holocene surface rupturing earthquakes (Fig. 2a; e.g., Johnson et al., 2001; Personius et al., 2014; Morell et al., 2018; Schermer et al., 2021; Harrichhausen et al., 2023). Two of these faults, the Leech River and Devils Mountain faults, form a continuous ~W-striking fault system (LRDM) that dips steeply north (Johnson et al., 2001; Li et al., 2018a), and transects the majority of the onshore Cascadia forearc across southern Vancouver Island in Canada, and the San Juan Islands and Puget Lowland in Washington State (Fig. 2). We chose to use this structure to model megathrust-coupling induced slip and help constrain the driving force of permanent deformation in northern Cascadia because of its wide transect and relatively long paleoseismic record spanning the Holocene (e.g., Johnson et al., 2001, 2004a; Personius et al., 2014; Morell et al., 2017, 2018; Barrie and Greene, 2018; Harrichhausen et al., 2021).

2.1 Paleoseismic studies

Paleoseismic studies along the LRDM, summarized in Table 1 and denoted with letters i–vi on Fig. 2a, indicate this structure has hosted at least five surface rupturing earthquakes with oblique slip in the Holocene. Evidence for surface-rupturing earthquakes is present as offset Quaternary sediments and offset subaqueous banks observed in bathymetry along the eastern WNW-striking portion of the Leech River fault on southern Vancouver Island (Morell et al., 2017, 2018; Harrichhausen et al., 2021), and along the Devils Mountain fault offshore of Victoria, British Columbia and in Washington State (Johnson et al., 2001, 2004a; Personius et al., 2014; Barrie and Greene, 2018). Paleoseismic trenching, geomorphic mapping, and stratigraphic analyses consistently indicate N-side-up motion along both faults (Table 1). Right-lateral offset of the LRDM is documented in paleoseismic trenches and by offset banks at three locations (ii, iii, and v), with the most unambiguous observation of strike-slip kinematics along the Devils Mountain fault where Personius et al. (2014) used 3D trenching to show right-lateral offset of glacial outwash channels and older bedrock faults. In contrast, left-lateral offset is documented in a paleoseismic trench excavated across a southward branch of the Devils Mountain fault, the Utsalady Point fault (vi). Earthquake rupture ages and dated offset stratigraphy suggest a minimum slip-rate of 0.05 mm/yr and a maximum of 1.6 mm/yr, with no spatial pattern in minima and maxima observed along strike of the fault system (Fig. 2b; Table 1). No evidence for Holocene surface rupture of the western-most W-striking section of the Leech River fault has been observed, and this portion of the fault has been considered inactive due to the observation of Oligocene marine sediments nonconformably overlying the fault on the west coast of Vancouver Island (MacLeod et al., 1977; Fairchild and Cowan, 1982; Groome et al., 2003). However, pronounced topographic lineaments following the bedrock surface trace of this portion of the fault and dense vegetation potentially obscuring exposures of faulted Oligocene sediments, may suggest more recent fault slip (Morell et al., 2017).

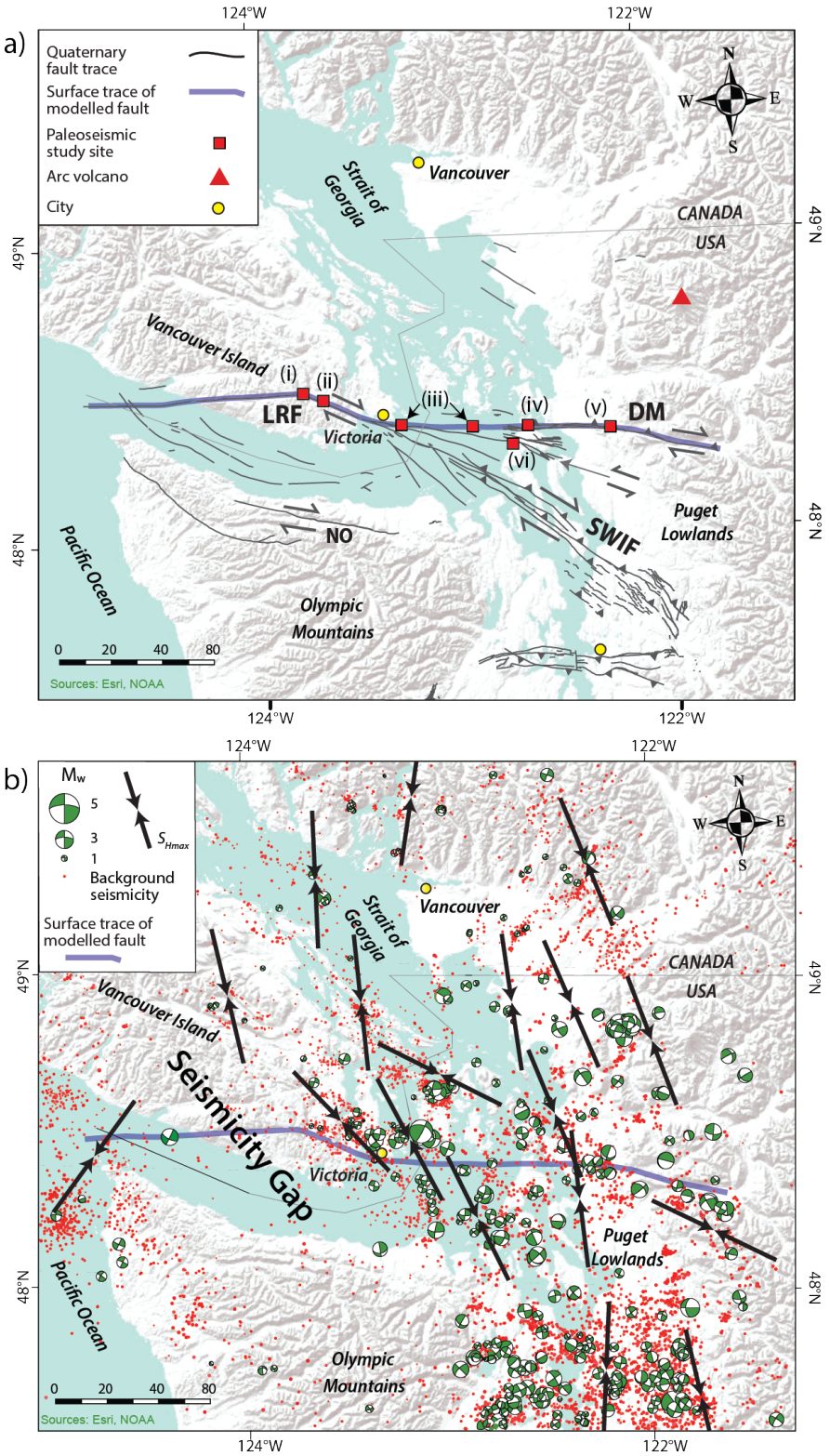

Figure 2 a) Surface traces and kinematics of Quaternary–Active crustal faults in northern Cascadia highlighting the Leech River (LRF) and Devils Mountain (DM) faults, combined to make the Leech River-Devils Mountain fault system (LRDM). Paleoseismic study results and references (locations shown as red boxes i–vi) are shown in Table 1. Fault traces are from the United States Geological Survey (USGS) Quaternary fault and fold database. Quaternary reverse slip has been observed on the Seattle fault zone (SFZ) (Johnson et al., 1994, 1999; Nelson et al., 2003; Blakely et al., 2002), right-lateral slip on the North Olympic fault zone (Nelson et al., 2017; Schermer et al., 2021), and right-lateral oblique slip on the southern Whidbey Island fault zone (SWIF) (Johnson et al., 1996; Sherrod et al., 2008). b) Upper plate crustal seismicity (< 35 km depth) in northern Cascadia from January 1, 1970 through April 29, 2015 compiled by Brocher et al. (2017) from the Pacific Northwest Seismic Network (2022). S_{Hmax} directions calculated by Balfour et al. (2011) from clusters of crustal earthquake focal mechanisms are shown by black arrow pairs. Adapted from Harrichhausen et al. (2021).

Fault	Location	Type	Fault dip	Kinematics	Slip rate	Earthquake ages	Reference
LRF	i	Geo-morphology	Subvertical	N-side up	N/A	N/A	Morell et al. (2017)
LRF	i	Trench	Subvertical	N-side up	0.2-0.3 mm/yr (vertical slip)	$1.7 \pm 0.1, 2.2 \pm 0.1, 8.7 \pm 0.3$ ka	Morell et al. (2018)
LRF	ii	Trench	Subvertical	Oblique right-lateral	N/A	9.4 ± 3.4 ka	Harrichhausen et al. (2021)
DMF	iii	Bathymetric, seismic reflection data	Subvertical	Oblique right-lateral	$0.8 - 1.3$ mm/yr	N/A	Barrie and Greene (2018)
DMF	iv	Well logs	$45° - 75°$ N	N-side up	$0.05 - 0.30$ mm/yr (vertical)	N/A	Johnson et al. (2001)
DMF	v	Trench	subvertical to N-dipping	Oblique right-lateral	0.14 ± 0.1 mm/yr (strike slip)	$2.2 \pm 0.1, 8.1 \pm 0.1$ ka	Personius et al. (2014)
UPF	vi	Trench	Subvertical	Oblique left-lateral	Mininimum slip rate $= \sim 1.6$ mm/yr	$100 - 400, 1100 - 2200$, cal B.P.	Johnson et al. (2004a)

Table 1 Summary table of paleoseismic studies of the Leech River (LRF) and Devils Mountain (DMF) and Utsulady Point (UPF) fault systems

2.2 Crustal seismicity and forearc stress field orientations

In northern Cascadia, instrumental crustal seismicity (located at < 35 km depth, recorded by the Pacific Northwest Seismic Network between 1970–2015, Brocher et al., 2017) is concentrated in a region along the eastern Leech River fault and the Devils Mountain fault (Fig. 2b). In comparison, reduced seismicity along the western Leech River fault (Fig. 2b) may suggest lower strain rates, which is consistent with this portion of the fault being inactive. However, crustal seismicity increases again towards the trench from the onshore portion of the western Leech River fault, resulting in a 'seismicity gap' where there is the reduction in seismicity between the inner forearc and the offshore portion of the forearc (Fig. 2b; Brocher et al., 2017; Bostock et al., 2019). Seismicity relocated on the eastern WNW-striking portion of the Leech River fault suggests that it is a $\sim 60°$ N-dipping zone of subvertical en échelon faults extending to a depth of ~ 28 km (Li et al., 2018a).

Earthquake focal mechanisms along the LRDM predominantly show right-lateral slip on steeply dipping W–NW striking fault planes, and N–S shortening on reverse faults (Fig. 2b; Brocher et al., 2017; Li et al., 2018a). These focal mechanisms are consistent with oblique right-lateral slip observed in paleoseismic studies at sites ii, iii, and v (Table 1). NNW–SSE maximum horizontal compressive stress (S_{Hmax}) and σ_1 directions along the fault system, derived from clusters of crustal seismicity by Balfour et al. (2011), would also predict that the LRDM accommodates oblique reverse right-lateral slip if the observed stress was relieved by these faults (Fig. 2b). However, the S_{Hmax} direction derived for the upper crust offshore the western end of the Leech River fault would predict a left-lateral component to slip (Fig. 2b).

2.3 GNSS derived upper plate strain

A combination of GNSS velocity vectors, geologic slip rates, paleomagnetic declination anomalies, seafloor spreading rates, and earthquake slip vector analyses together have been used to produce block models of northern Cascadia that predict rates and kinematics on active forearc faults (McCaffrey et al., 2007; Evans, 2022). These models separate the Pacific northwest region of North America, which encompasses the Cascadia subduction zone, into regions of relatively cohesive, rigid blocks. The Devils Mountain fault is one of the block boundaries and the McCaffrey et al. (2007) block model predicts ~ 0.4 mm/yr of right-lateral normal slip along this structure. The strike-slip component of this slip-rate is consistent with both paleoseismic studies and crustal seismicity. However, the 70% confidence interval error ellipse for this vector is large ($>> 0.4$ mm/yr) and a left-lateral reverse slip vector is within its bounds. The Evans (2022) block model discretizes slip rates and kinematics along this boundary, and predicts $\sim$ 0.05 to 0.5 mm/yr of reverse right-lateral slip along the Devils Mountain fault. The lowest slip-rates, and the most substantial component of reverse slip, occur near the intersection between the South Whidbey Island fault zone and the Devils Mountain fault and increase to $\sim$0.5 mm/yr towards the west and $\sim$ 0.2 mm/yr to the east. Again, the model-derived standard deviations of these slip rates are larger than the absolute values of the vectors ($\sim$ 0.1 to 1.0 mm/yr), indicating that opposite slip kinematics are within the error bounds of the model.

GNSS velocities collected throughout the past several decades also suggest N–S shortening across the Olympic Mountains, which has been interpreted to result from a northward-migrating southern Cascadia forearc (Khazaradze et al., 1999; Mazzotti et al., 2002). Oroclinal bending, reflected by counterclockwise rotation of the northern forearc and clockwise rotation of the southern forearc about an axial trace that bisects the Olympic Penin-

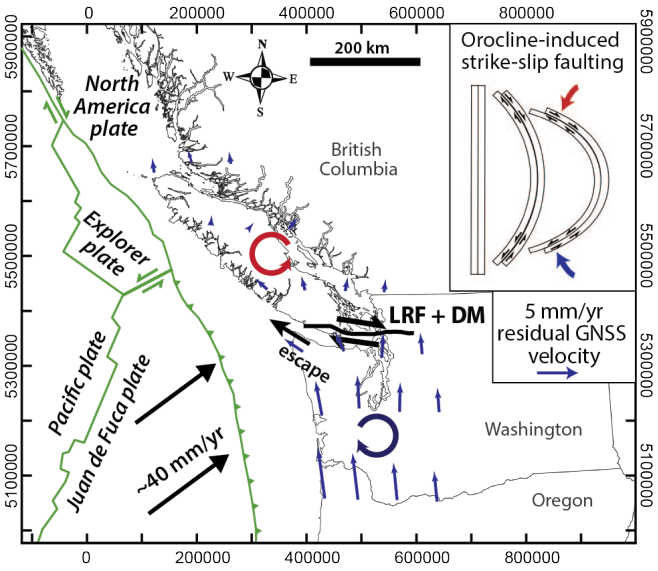

Figure 3 Map showing the tectonic processes of Cascadia that may influence right-lateral slip on the LRDM. Clockwise rotation and northward motion of the southern Cascadia relative northern Cascadia induces oroclinal bending and westward escape of the northwest Olympic Peninsula and western Vancouver Island (Nelson et al., 2017; Finley et al., 2019; Harrichhausen et al., 2021). Inset shows how oroclinal bending results in strike-slip faulting on each limb of the orocline, similar to flexural slip on a fold. Small blue arrows show gridded interpolation of the residual GNSS velocity field with respect to stable North America from (Mazzotti et al., 2011) and indicate west–northwestward escape of the Olympic Peninsula and western Vancouver Island. Relative plate motion from (DeMets et al., 2010). Clockwise rotation shown in blue and counterclockwise rotation shown in red. UTM grid coordinates (m) are in NAD83 UTM Zone 10N.

sula (Fig. 3; Miller et al., 2001; Mazzotti et al., 2003; McCaffrey et al., 2007; Finley et al., 2019), has been suggested to accommodate this shortening (Finley et al., 2019; Harrichhausen et al., 2021). Paleomagnetic and structural geology studies suggest oroclinal bending has been ongoing since 18 Ma (Wells and McCaffrey, 2013; Finley et al., 2019). Right-lateral fault slip on E–W-striking faults in northern Cascadia is suggested to result from deformation similar to flexural slip on a fold limb, during oroclinal bending (Fig. 3; Finley et al., 2019; Harrichhausen et al., 2021).

GNSS residual velocities, where the estimated elastic effect of subduction zone coupling is removed from total GNSS velocities, have also been used to constrain permanent forearc deformation in Cascadia (Khazaradze et al., 1999; Miller et al., 2001; Mazzotti et al., 2003, 2011). These residuals are based on subduction zone coupling models and the lack of constraint on coupling (e.g., Wang et al., 2003; Wang and Tréhu, 2016) may inhibit their usefulness. However, some areas of the residual velocity fields predict forearc deformation that is consistent with observed forearc fault kinematics (Harrichhausen et al., 2021). GNSS residuals predict northwestward motion, or "escape", of the Olympic Peninsula and the west coast of Vancouver Island relative to stable North America (Mazzotti et al., 2002, 2011), which, along with oroclinal bending, may accommodate the observed N–S shortening across the Olympic Peninsula (e.g., Nelson et al., 2017; Finley et al., 2019; Harrichhausen et al., 2021). This trenchward extrusion of the forearc would also imply right-lateral slip on the Leech River fault as the portion of Vancouver Island south of the Leech River fault is moving west with respect to the northern side of the fault (Fig. 3). Towards the east along the Devils Mountain fault, a south-to-north reduction in northward residual velocities suggests N–S shortening perpendicular to the strike of the Devils Mountain fault (Fig. 3; Khazaradze et al., 1999; Mazzotti et al., 2002, 2011), predicting reverse slip on the eastern segment of our modelled fault system.

3 Model description

We used a 3D BEM model (e.g., Crouch and Starfield, 1983; Thomas, 1993; Loveless et al., 2010; Delano et al., 2017; Duckworth et al., 2021) to calculate stress in a linear elastic half-space representing the upper plate of the Cascadia subduction zone (based on algorithms in Meade, 2007). The stress results from prescribed slip rates on the subduction zone interface that mimic interseismic coupling, coseismic megathrust rupture, and partitioned forearc strain. To estimate the slip rates on the LRDM and associated faults, we calculated slip rates on meshes representing these faults that are required to relieve the stress induced by the tractions prescribed on the subduction zone mesh. This model has previously been used to estimate slip on other crustal forearc structures in the Cascadia forearc in Washington State (Delano et al., 2017; Duckworth et al., 2021; Loveless, 2021). We adapted the model to include the faults in our study area, and to test how partitioned strain is accommodated by forearc faulting (archived model files available in: Harrichhausen et al., 2024).

The inputs to the BEM model are: A meshed surface representing the Cascadia subduction zone with prescribed dip-slip and strike-slip rates representing interseismic coupling, partitioned interseismic coupling, or coeseismic rupture (Delano et al., 2017); A meshed surface(s) representing forearc fault(s); Coefficients and assumptions governing the elastic properties of the half-space (Poisson's ratio and shear modulus). The meshed surfaces are discretized as triangular dislocation elements (TDEs) for which slip rates are prescribed or calculated individually. This discretization allows for complex surface geometries, and spatially variable coupling and slip-rate distributions on the modelled structures.

3.1 Subduction zone mesh

The Cascadia subduction zone mesh and slip-rates are from Delano et al. (2017), with the subduction zone geometry based on slab contours from McCrory et al. (2006). Each TDE of the mesh is defined by its own strike and dip based on the slab contours, and these orientations are used to resolve the strike-slip and dip-slip components of deformation. The slip rates on the Cascadia subduction zone mesh equate to the slip-deficit, or the rate of potential elastic slip accumulated on the

subduction interface due to coupling in mm/yr. These slip deficit values have been calculated using a geodetically constrained block model that uses a GNSS velocity field consisting of 1717 stations, in conjunction with independently (geologically) calculated relative block motions to predict slip on the block boundaries (Meade and Loveless, 2009; Delano et al., 2017). This block model uses potentially active faults as block boundaries, and includes a block boundary that is close to our mapped trace of the LRDM. The coupling model resolves ~ -13 to 35 mm/yr of dip-slip deficit and ~ -35 to 10 mm/yr strike-slip deficit on the subduction zone interface, where positive slip rates are reverse and left-lateral, respectively. The greatest coupling is located where the subducting slab geometry changes from ~N-striking to ~NW-striking at UTM 530000 m N and the slab dip is reduced (Fig. 4a). At this location, the strike-slip deficit also changes from right-lateral to left-lateral from south to north due to a change in the obliquity of subduction that occurs at the same location. At the southern extent of the modelled slab, the Delano et al. (2017) model prescribes an excess of dip slip on the subduction interface (i.e., where the slip deficit is negative). The negative slip deficit here has also been described by other coupling models and it may result from forearc GNSS velocities in this region being significantly influenced by complex interactions with the Mendocino triple junction (e.g., Saux et al., 2022). This region is far enough away (> 500 km) from the LRDM that it likely has little impact on our results. More details on the block model used to calculate the slip deficit and the Cascadia subduction zone mesh used in our model are described in Delano et al. (2017) (Supplementary Material).

We prescribed three different slip rate distributions to the subduction zone mesh to predict slip rates on the LRDM due to unpartitioned interseismic coupling (Model A), interseismic strike-slip coupling (to model partitioned forearc strain, Model B), and coseismic megathrust rupture (Model C). For Model A, we prescribe a negative (normal) slip-deficit rate and a corresponding left- or right-lateral slip-deficit rate in the opposite direction of relative plate motion (Fig. 4a, b). These slip deficit rates imposed on the upper plate mimic the dragging of the upper plate along the subduction interface during interseismic coupling. To model partitioned forearc strain (Model B), we prescribe zero dip-slip deficit rates to the subduction zone mesh, thus only the strike-slip deficit rates remain as model inputs that deform the elastic half-space. Finally, to model coseismic megathrust rupture (Model C), we prescribe a positive (reverse) slip rate and a corresponding strike-slip rate parallel with relative plate motion (Fig. 4c, d), mimicking the full elastic recovery of the upper plate during, or immediately after, a rupture of the entire Cascadia subduction zone.

3.2 Forearc fault meshes

We constructed the meshed surface representing the LRDM by extrapolating surface traces of the faults at a specified dip to a maximum depth. The surface traces in Washington State were interpolated from Johnson et al. (2001); Personius et al. (2014); Greene et al. (2018), Personius et al. (2014), and Greene et al. (2018). The trace of the Leech River fault is based on geomorphic mapping from Graham (2018), Morell et al. (2017, 2018), and Harrichhausen et al. (2021), as well as geologic mapping of the fault from Massey et al. (2005). We also extended the Leech River fault ~ 40 km offshore to the west based on a map of the Leech River fault by MacLeod et al. (1977). Although this portion of the fault may not be active (MacLeod et al., 1977; Fairchild and Cowan, 1982; Groome et al., 2003), S_{Hmax} orientations have been calculated from crustal seismicity in this region (Balfour et al., 2011), providing observations to compare to our modelled fault kinematics. We extracted UTM coordinates (NAD83 Zone 10N) from the vertices of these surface traces and used a published MatLab script (available at https://github.com/jploveless/meshing) to produce a mesh constructed from 3000 m sided triangles. We used a depth of 28 km and a dip of 60° N for the fault system based on relocated seismicity on the Leech River fault from Li et al. (2018a).

We also use three additional multi-fault models using the same subduction zone slip rate distributions as Models A–C: Model D–interseismic coupling, Model E–partitioned interseismic coupling, and Model F–coseismic rupture. These multi-fault models include the eastern Leech River fault, the Devils Mountain fault, Utsalady Point fault (Johnson et al., 2004b), Strawberry Point fault (Johnson et al., 2001), and the South Whidbey Island fault (Johnson et al., 1996; Sherrod et al., 2008). The purpose of including the additional fault zones was to test how multiple structures interact with each other. We chose to include these faults as their surface traces all converge towards each other. We also chose to exclude the western W-striking segment of the Leech River fault in this model, as there is no reported evidence of offset Upper Oligocene sediments that overlie this segment of the fault on the west coast of Vancouver Island (MacLeod et al., 1977; Fairchild and Cowan, 1982; Groome et al., 2003), and we wanted to test how removing this portion of the fault would affect its kinematics. We limited the down-dip projection of each fault to 20 km and set them all to dip 75° towards the north or northwest. We used these new parameters to ensure that the surfaces did not cross-cut one another.

3.3 Elastic half-space assumptions

The BEM model employs the prescribed slip deficit rate distributions to analytically calculate the stress rate at a given point in a linear, homogeneous elastic half-space, characterized by a Poisson's Ratio of 0.25 and shear modulus of $3\text{x}10^8$ Pa. The BEM model then predicts slip-rates on crustal faults by solving for the slip-rate on each crustal fault TDE required to completely relieve the stress rate on a traction-free surface at that point in the elastic half-space. Displacement normal to any of the TDEs is not allowed in the model to prevent fault opening. The model assumes a linear homogeneous crust, and that the crustal faults are traction-free surfaces that relieve all of the stress imposed on them, including the

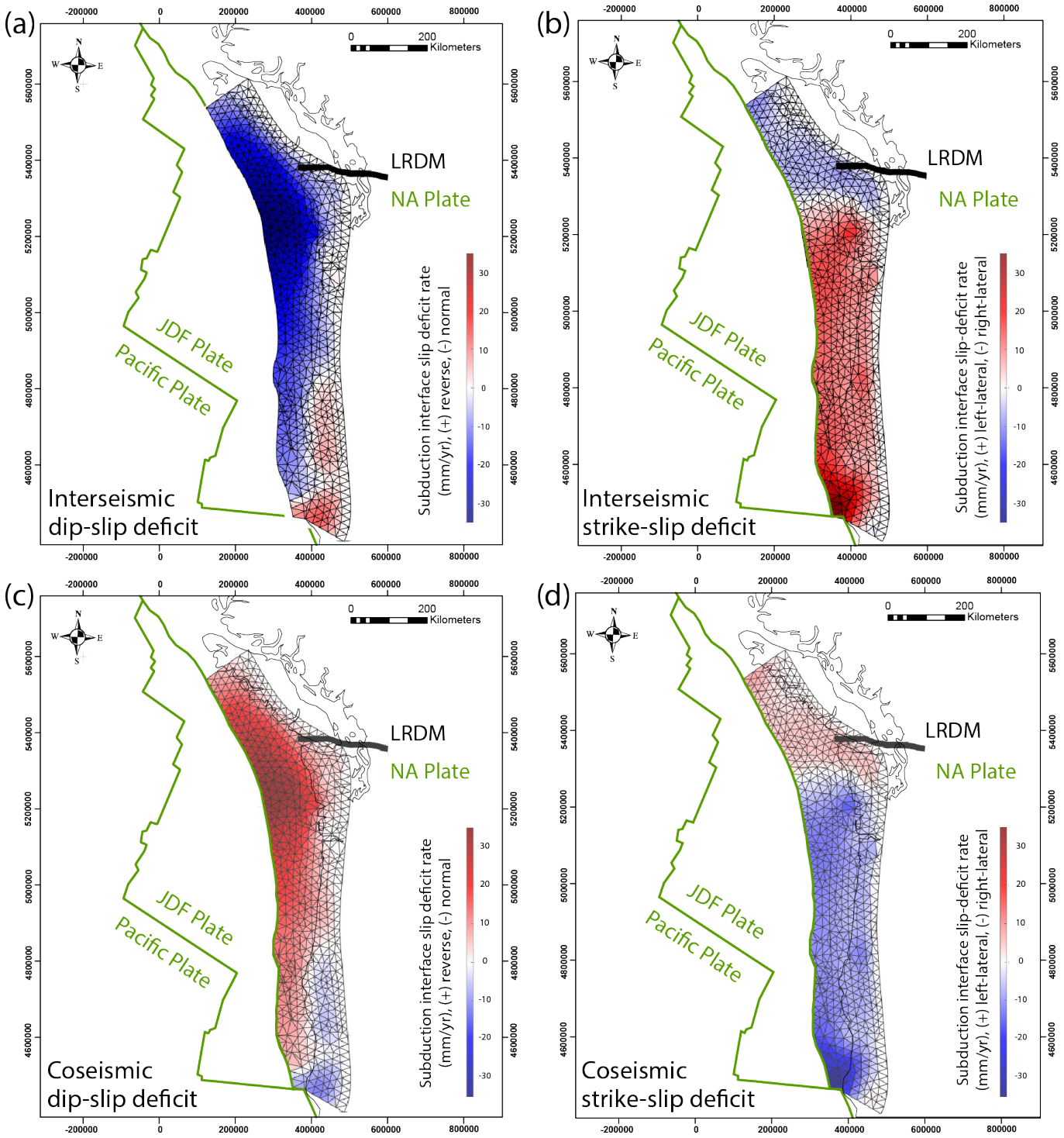

Figure 4 Prescribed slip rates (tractions) on a mesh representing the Cascadia subduction zone interface that drive elastic deformation and forearc fault slip in the boundary element method (BEM) model. Interseismic dip-slip (a) and strike-slip (b) deficit rates represent interseismic coupling. Coseismic dip-slip (c) and strike-slip (d) rates represent coseismic slip. The mesh representing the Leech River-Devils Mountain forearc fault system (LRDM) is shown in black, and the Juan de Fuca (JDF), North America (NA), and Pacific plate boundaries are shown in green. UTM grid coordinates (m) are in NAD83 UTM Zone 10N. Input slip deficit and slip rates are from (Delano et al., 2017).

stresses induced by slip on neighboring TDEs on the same or neighboring faults. Therefore, where we model multiple crustal faults, the slip rates are lower where the faults are in close proximity to each other as the strain is distributed. Additionally, slip rates are lower at the edges of the faults where there are no free surfaces. The model does not take into account viscous deformation below the brittle-ductile transition, changes of fluid pore pressure, or fault slip mechanics and earthquake recurrence intervals. However, the simplicity of the model allows us to conduct a first-order test of whether stress due to elastic deformation of the forearc by megathrust coupling or rupture, results in the observed fault kinematics along the LRDM.

4 Model Results

Model A, where unpartitioned coupling on the Cascadia subduction interface (including both the strike-slip and dip-slip components) drives strain in the upper plate, predicts reverse left-lateral slip along the entire LRDM (Fig. 5a). Reverse slip rates range from ~ 0 to 3 mm/yr with the highest rates at the far western end of the Leech River fault, and where the Leech River fault bends and strikes WNW. This western increase in slip rate is partially due to higher slip rates being produced where the fault is located closer to the subduction interface. Left-lateral strike slip rates range from ~ 0 to 3.5 mm/yr with a steady increase in slip rates towards the western end of the fault system, again due to proximity to the subduction interface. Strike-slip rates decrease down-dip on the LRDM mesh away from the Earth's surface.

Model B, where the prescribed strike-slip deficit rates on the megathrust mimic partitioned forearc strain, predicts that the LRDM accommodates left-lateral (red) slip, and both normal (blue) and reverse (red) components of dip slip (Fig. 5b). Modelled dip-slip rates range from ~ 0.6 mm/yr of normal slip on the W-striking western end of the Leech River fault to ~ 0.15 mm/yr of reverse slip along the W-striking Devils Mountain fault. Very little to no slip is calculated on the NW-striking middle segment of the fault system, except for one $\sim$ 5 km section in the middle of this segment where < 0.1 mm/yr of reverse slip is estimated. Modelled strike-slip rates are also lower for the partitioned coupling model: ~ 0 to 0.7 mm/yr of left-lateral strike slip with the rate decreasing towards the east away from the subduction zone. The overall reduction in slip-rates are expected due to the lower absolute value of the slip deficit rates prescribed on the subduction interface.

In Model C (Fig. 5c), coseismic rupture on the megathrust results in calculated slip-rate distributions for the LRDM that are the opposite of Model A. Instead of reverse left-lateral slip, normal and right-lateral slip with slip rates ranging from ~ 0 to 3 mm/yr increasing towards the western end of the Leech River fault are predicted.

In Models D–F (Fig. 6), where we include multiple faults (the eastern Leech River, Devils Mountain, South Whidbey Island, Strawberry Point, and Utsalady Point faults), we see similar slip-rate distributions compared to the previously described models that only include the LRDM. In all of the multi-fault models, slip rates are lower where the faults overlap each other (they are subparallel in space) and deformation is partitioned onto multiple surfaces. Also, the NW-striking South Whidbey Island fault has greater slip rates than the the more westerly-striking Utsalady Point, Strawberry Point, and Devils Mountain faults. In Model D, where unpartitioned interseismic coupling drives strain, all of the modelled faults are predicted to accommodate < 0.7 mm/yr of reverse dip slip and < 1.6 mm/yr of left-lateral slip. Model E, where only strike-slip coupling drives deformation, predicts < 0.45 mm/yr of left-lateral slip on the forearc faults. The far-eastern down-dip portion of the Leech River fault, and where the Leech River fault overlaps with the South Whidbey Island fault, show < 0.05 mm/yr of normal slip while the rest of the faults show < 0.2 mm/yr of reverse slip. Finally, in Model F, coseismic rupture on the megathrust drives the opposite kinematics of the interseismic coupling model (Model D), with < 0.7 mm/yr of normal slip and < 1.6 mm/yr of right-lateral slip.

5 How do the BEM models compare with previous studies?

Our models of upper plate fault kinematics indicate that the elastic response of the upper plate to subduction zone coupling, or coseismic rupture, cannot be the sole explanation for the permanent deformation accommodated by the modelled upper plate faults in northern Cascadia. Predominantly left-lateral reverse slip predicted in the interseismic models (Models A, B, D, and E) differs in strike-slip sense from the right-lateral fault kinematics inferred on these structures in paleoseismic studies (Fig. 2a, Table 1a), instrumental seismicity (Fig. 2b), and geodetic block modelling. The coseismic models (Models C and F) predict normal slip, which is not inferred for any of the structures in this study. In contrast to these inconsistencies, the single fault interseismic coupling model (Model A) and instrumental seismicity suggest similar reverse left-lateral strain regimes off the west coast of Vancouver Island, and may indicate subduction zone coupling is an important driver of faulting in the outer forearc.

5.1 Paleoseismic studies

The fault kinematics produced in the BEM models are inconsistent with most of the observed active kinematics from paleoseismic studies of the LRDM, whether it is modelled as a single structure (Models A-C) or multiple faults (Models D-F). Paleoseismic investigations predominantly observe reverse right-lateral slip aside from a study on the Utsalady Point fault (Fig. 2a; Table 1). These observations are in contrast with the single structure and multi-fault unpartitioned interseismic coupling models predicting reverse left-lateral slip on all faults (Models A and D). In the strain partitioning model (Model B), the sense of dip slip switches along the western portion of the Leech River fault. However, as Model B still predicts left-lateral slip along the length of the fault, it is still inconsistent with the paleoseismic observations. Finally, both the coseismic models (Models C and F) produce right-lateral slip on all forearc faults, similar to paleoseismic observations (Fig. 2a; Table 1). However, they also predict normal slip on N-dipping faults, inconsistent with the observed N-side up motion along the LRDM.

Despite the inconsistencies between the BEM models and paleoseismic observations in slip sense, most of the modelled absolute slip rates compare relatively well with most of the observed slip rates (Table 1). Model B, and Models D through F estimate absolute slip rates (0 to 1.5 mm/yr) that are similar to the slip rates observed in paleoseismic studies. Given this similarity, we speculate that the paleoseismic slip sense observations could incorporate alternating slip histories result-

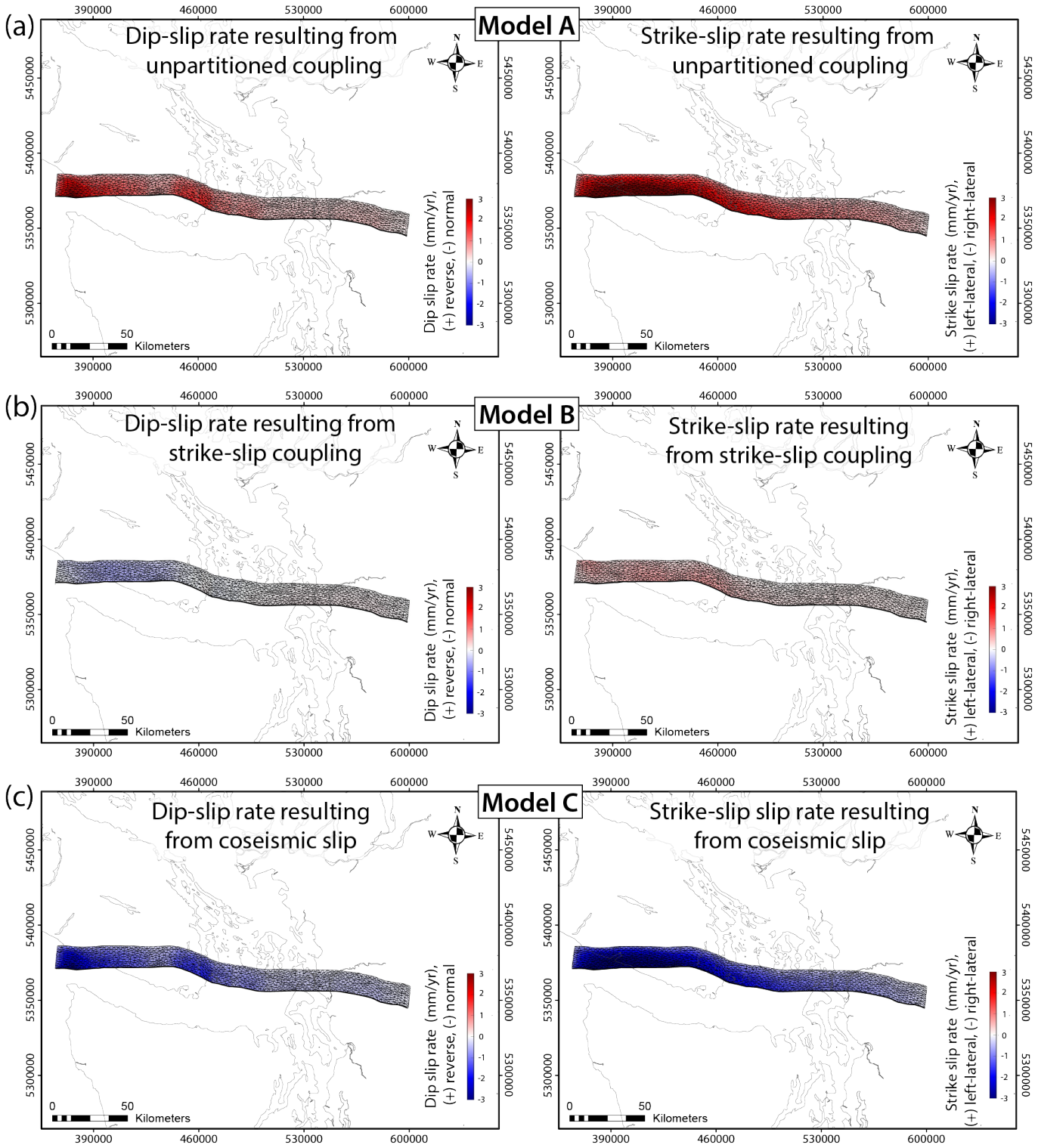

Figure 5 Dip-slip and strike-slip rates on the LRDM resulting from unpartitioned coupling in Model A (a), strike-slip coupling in Model B (b), and coseismic slip in Model C (c) on the Cascadia subduction zone mesh (Fig. 4). Red denotes reverse slip-rates and left-lateral slip rates, while blue denotes normal slip rates and right-lateral slip rates. Surface trace of the LRDM shown with solid black line. Fault dips away from the surface trace to the north. UTM grid coordinates (m) are in NAD83 UTM Zone 10N.

ing from stress reversals during the megathrust cycle (e.g., Hasegawa et al., 2012; Regalla et al., 2017; Cortés-Aranda et al., 2022), and the kinematics observed today are the net sum of these alternating slip sense events. This hypothesis could explain why left-lateral slip sense is observed on the Utsulady Point fault in contrast to right-lateral slip sense or pure dip slip along the rest of the fault system along strike, such as the Devil's Mountain Fault (Fig. 2a; Table 1). Although this possibility exists, the most unambiguous observation of strike-slip displacement are right-laterally offset channels observed in 3D trenching along the Devils Mountain fault (Personius et al., 2014), and the oblique right-lateral slip is consistent with interseismic GNSS and seismicity ob-

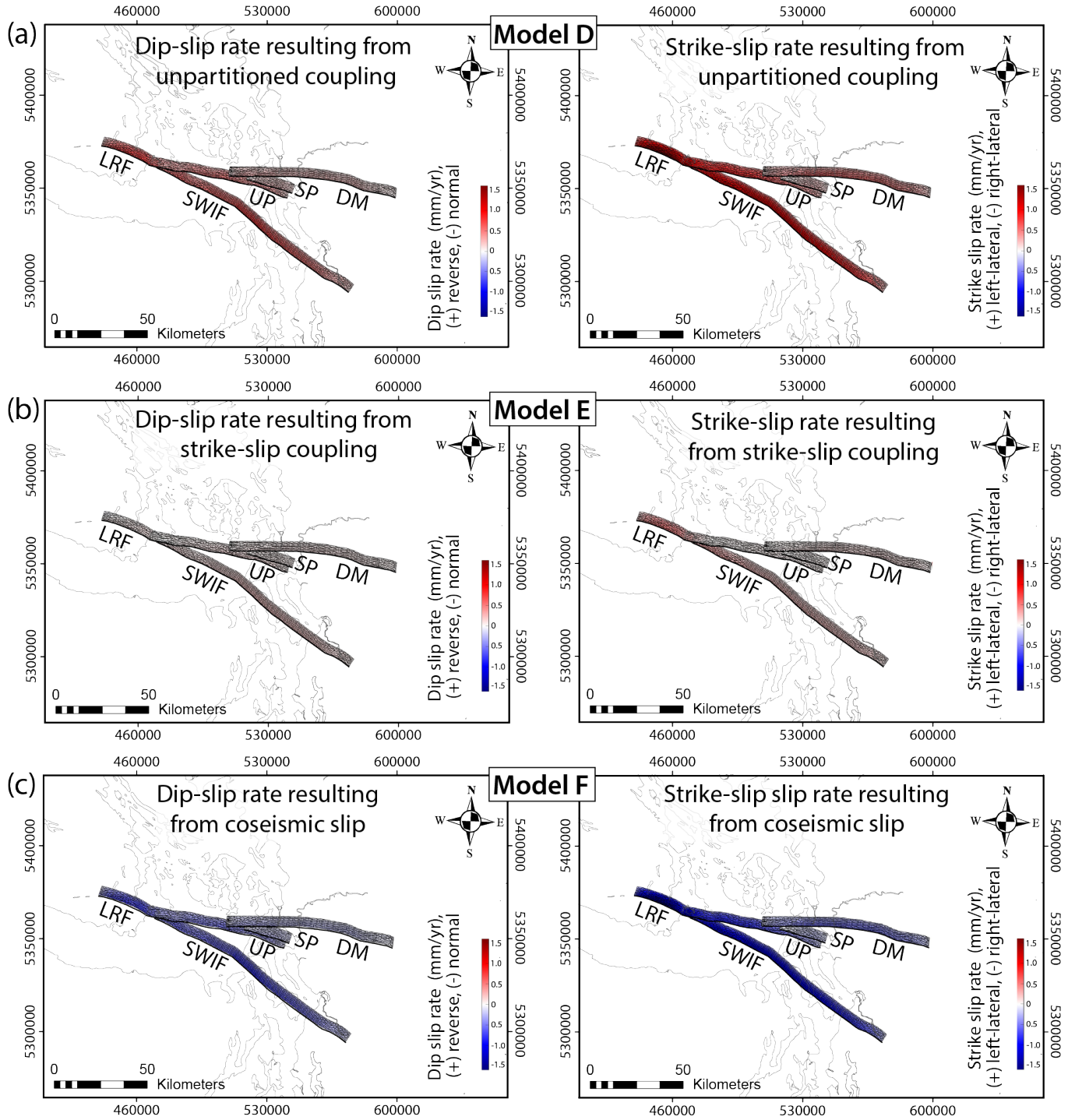

Figure 6 Maps showing modelled dip-slip (left) and strike-slip (right) rates on on multiple faults in the northern Cascadia forearc. Slip in the models results from unpartitioned coupling in Model D (a), only strike–slip coupling in Model E (b), and unpartitioned coseismic slip in Model F (c) on the Cascadia subduction zone mesh (Fig. 4). Red denotes reverse slip-rates and left-lateral slip rates, while blue denotes normal slip rates and right-lateral slip rates. Modelled faults are the eastern Leech River (LRF), Devils Mountain (DM), Strawberry Point (SP), Utsalady Point (UP), and South Whidbey Island (SWIF) faults. Surface trace of the crustal faults are shown with solid black lines. Faults dip away from the surface trace to the north. UTM grid coordinates (m) are in NAD83 UTM Zone 10N.

servations (Fig. 2b; Fig. 3). This consistency between trenching and interseismic observations is indicative that permanent interseismic strain is right-lateral, and is in contrast with all of our interseismic BEM models (Models A, B, D, E). Finally, Models A and C predict maximum slip rates of up to 3 to 3.5 mm/yr at the western end of the LRDM, which have not been observed in paleoseismic investigations. In fact, these highest modelled slip rates occur where the LRDM is thought to be inactive (MacLeod et al., 1977; Fairchild and Cowan, 1982; Groome et al., 2003). Thus this inconsistency may be further evidence that our simple model of elastic deformation resulting from the megathrust cycle cannot be used to explain the observed forearc faulting in northern Cascadia.

5.2 Crustal seismicity

Similar to the paleoseismic observations, recorded crustal seismicity, which has occurred during an interseismic period in the Cascadia subduction zone megathrust cycle, is also inconsistent with the BEM models of inner forearc (onshore) fault kinematics. Upper plate focal mechanisms (Brocher et al., 2017; Li et al., 2018a) and S_{Hmax} directions derived from crustal seismicity (Balfour et al., 2011) predict right-lateral reverse slip along the LRDM (Fig. 2b). This reverse right-lateral slip is inconsistent with the interseismic coupling models (Models A, B, D, and E) that predict a left-lateral component of strike slip along the modelled upper plate faults, as well as the coseismic BEM models (Models C and F) that yield a normal component of dip slip on these structures.

In contrast to the inner forearc, the reverse left-lateral slip predicted by our unpartitioned interseismic coupling model (Model A) in the outer forearc off the west coast of Vancouver Island is consistent with S_{Hmax} directions derived from upper plate seismicity in the same region. At the farthest west end of the Leech River fault, off the west coast of Vancouver Island, the SW–NE S_{Hmax} direction from crustal seismicity would predict left-lateral reverse slip on a W-trending fault (Fig. 2b), consistent with slip produced by our unpartitioned interseismic coupling model (Model A). Although the western on-land portion of the Leech River fault has formerly been deemed inactive (MacLeod et al., 1977; Fairchild and Cowan, 1982; Groome et al., 2003), crustal seismicity increases offshore towards the west (Fig. 2b), suggesting the stress rate also increases offshore (Stevens and Avouac, 2021), and potentially indicates offshore active faulting. There is no evidence that this offshore faulting is along the Leech River fault. However, our interseismic model shows left-lateral oblique slip on a W-striking fault, which implies the same SW–NE S_{Hmax} direction as calculated by Balfour et al. (2011). This SW–NE S_{Hmax} direction is consistent with inferred kinematics on seismically imaged structures in the forearc basin sediments west of Vancouver Island. The imaged structures are late Pliocene NE-verging reverse faults and folds (Hayward and Calvert, 2007) and may still be active. This area west of Vancouver Island is immediately above where coupling on the megathrust increases towards the trench (Schmalzle et al., 2014; Li et al., 2018b, Fig. 4a, b;). We speculate that these observations indicate subduction zone coupling may be important in controlling permanent strain in the outer forearc closer to the trench, which is proximal or immediately above the locked portion of the megathrust.

5.3 GNSS derived strain and previous BEM modelling

Geodetic block models of Cascadia use GNSS velocities to constrain the relative rotations of microplates, interseismic elastic deformation due to locked faults along microplate boundaries, and the distribution of coupling along partially locked faults. Slip rates are calculated using the difference between the rotation rates at the block boundaries (Meade and Loveless, 2009; Evans, 2022). Thus, these models represent an inversion of the GNSS velocities, while our model "drives" forearc deformation using the stress that results from subduction zone coupling. As the block models are inferred to be a prediction of the current deformation being observed at the block boundaries, they are a useful comparison with our modelled fault kinematics.

Two of the block models that include the Devils Mountain fault as a block boundary estimate right-lateral slip along this structure (McCaffrey et al., 2007; Evans, 2022), which is inconsistent with our prediction of left lateral slip on the Devils Mountain fault, the entire LRDM, or the network of forearc faults (Models A, B, D, and E). The McCaffrey et al. (2007) block model indicates a normal, right-lateral slip-rate slip rate of ~ 0.4 mm/yr on the Devils Mountain fault, consistent with our model driven by coseismic rupture (Model C). However, the McCaffrey et al. (2007) block model reflects interseismic GNSS velocities, and the error on the block model is large enough that left-lateral reverse slip is also possible. Therefore we hesitate to use this comparison to make any deductions about coseismic elastic deformation controlling permanent forearc deformation on this segment of our modelled fault system. Finally, the Evans (2022) block model predicts ~0.05 to 0.5 mm/yr (standard deviation of up to 1 mm/yr) of reverse right-lateral slip along the Devils Mountain fault, which is inconsistent with all of our models of upper plate fault kinematics.

6 What drives the observed oblique right-lateral slip?

Our BEM models suggesting that elastic response of the upper plate to interseismic subduction zone coupling and coseismic rupture alone cannot explain the observed fault kinematics of the LRDM may be representative of a larger area in Northern Cascadia. Similar BEM modelling by Duckworth et al. (2021) predicting slip on the North Olympic fault zone $\sim$ 50 km south of the Leech River fault (Fig. 1b), also concludes that stress arising from interseismic coupling does not drive the right-lateral oblique motion observed on this forearc fault zone. They suggest that coseismic strain may have resulted in reverse right-lateral slip; or, that the North Olympic fault zone acts as the northern boundary of a rotating tectonic block ("Olym" block, McCaffrey et al., 2013) and that strain along the boundary is the result of a deformation field larger than the subduction zone. Their coseismic BEM model, like ours, predicts normal slip and contrasts with the reverse slip that has been observed in paleoseismic studies (Schermer et al., 2021) and bedrock mapping (Polenz et al., 2004). Therefore, we conclude that these observations suggest coupling or coseismic rupture also do not drive fault slip on the Olympic Peninsula, and may indicate our results are not just confined to the LRDM and may reflect most of northern Cascadia.

Since our models indicate that subduction zone coupling and coseismic rupture alone cannot explain the observed strike-slip fault kinematics in the inner fore-

arc of northern Cascadia, we propose that permanent deformation accommodated by the LRDM combined is the combined effect of subduction zone processes and far-field tectonic processes. This interpretation is supported by the McCaffrey et al. (2007) and Evans (2022) block models, which predict right-lateral slip on the Devils Mountain fault and is in agreement with crustal seismicity and paleoseismic studies (Fig. 2). As these block models are based on GNSS data covering the entirety of the Pacific Northwest region (McCaffrey et al., 2007), they support our conclusion that including far-field deformation is needed to reproduce the observed fault kinematics in forearc strain models. Similar conclusions from studies of other subduction zones have been made where permanent inner forearc deformation is thought to reflect the background stress state of the forearc and is not directly related to subduction zone coupling (e.g., Townend and Zoback, 2006; Townend et al., 2012; Dimitrova et al., 2016).

A far-field tectonic process that we suspect is a substantial factor in driving forearc strain in northern Cascadia is the oroclinal bending of the Cascadia forearc, which accommodates north-south shortening across the Olympic Peninsula and may promote its westward escape (Fig. 3; Nelson et al., 2017; Finley et al., 2019; Harrichhausen et al., 2021). Right-lateral slip on the LRDM, in the case of oroclinal bending, is a result of flexural slip along the northern limb of the orocline (Fig. 3). Westward escape of the Olympic Peninsula relative to the northern forearc would also induce right-lateral motion on roughly west- and east-striking upper plate faults. Because residual GNSS velocities south of the Devils Mountain fault do not indicate westward escape immediately south of the Devils Mountain fault (Fig. 3), we suggest that the primary driver of right-lateral slip, at least at the eastern end of the LRDM, is flexural slip, while westward escape may explain right-lateral motion further west on the Leech River fault.

In addition to the previously described tectonic processes, we have not considered other drivers of forearc strain, such arc-parallel flow in the mantle wedge (e.g., Sternai et al., 2014; Chen et al., 2016) or buoyancy contrasts along the forearc (e.g., Rippke, 2020), that could potentially result in right-lateral slip along the LRDM fault. Although it is beyond the scope of this study, considering these other sources of forearc strain in future models is essential to determine what processes control permanent deformation of forearcs at different subduction zones.

7 Conclusions

Our BEM models suggest that elastic forearc strain from interseismic coupling would result in predominantly left-lateral reverse slip along the LRDM, and that elastic strain from coseismic megathrust rupture results in right-lateral normal fault slip. In addition, our models using only the strike-slip component of interseismic coupling to drive fault slip, mimicking forearc strain partitioning, also predict predominantly left-lateral forearc faulting. Multi-fault models predict the same fault kinematics as single fault models, albeit with lower slip rates, especially where faults are in close proximity to each other. These results are not consistent with paleoseismic studies, instrumental seismicity, and geodetic block models which predominantly indicate right-lateral, reverse fault kinematics on the modelled faults in northern Cascadia. This result allows us to deduce that observed permanent deformation in the inner forearc in northern Cascadia does not solely accommodate elastic strain driven by subduction coupling or coseismic rupture. S_{Hmax} directions predicting left-lateral slip along the furthest west, offshore portion of the modelled Leech River fault, are consistent with our interseismic coupling models. We speculate that this result suggests some of the elastic strain from subduction zone coupling may be reflected by permanent deformation in the outer forearc, closer to the coupled portion of the megathrust. In the inner forearc, we suggest that oroclinal bending, and west-northwestward extrusion of the Olympic Peninsula and the southwestern tip of Vancouver Island induce right-lateral slip on the LRDM.

Acknowledgements

Funding to support this research was from a Natural Sciences and Engineering Research Council of Canada (NSERC) Post Graduate Scholarship and Centre National d'Études Spatiale (CNES) postdoctoral fellowship to N. Harrichhausen, National Science Foundation Earth Sciences (NSF EAR) grants #1756943 and #2046278 to K. Morell, and #1756834 to C. Regalla. This manuscript benefited greatly from discussions on the tectonics of northern Cascadia with J. Loveless, E. Nissen, L. Lucinda, T. Finley, S. Bennett, E. Lynch, and E. Schottenfells. Finally we thank H. Tobin, E. Lindsay, and an anonymous reviewer for their thoughtful insight and comments on our manuscript.

Data and code availability

Codes and input files for the BEM models are available in Harrichhausen et al. (2024). These codes are adapted from Loveless (2021). GNSS velocity data in Fig. 1a is from https://www.unavco.org/software/visualization/GPS-Velocity-Viewer/GPS-Velocity-Viewer.html.

Competing interests

There are no competing interests pertaining to the authors.

References

Allmendinger, R. W. and González, G. Invited review paper: Neogene to Quaternary tectonics of the coastal Cordillera, northern Chile. *Tectonophysics*, 495(1-2):93–110, 2010. doi: 10.1016/j.tecto.2009.04.019.

Audet, P. and Bürgmann, R. Possible control of subduction zone slow-earthquake periodicity by silica enrichment. *Nature*, 510 (7505):389–392, 2014. doi: 10.1038/nature13391.

Balfour, N. J., Cassidy, J. F., Dosso, S. E., and Mazzotti, S. Mapping crustal stress and strain in southwest British Columbia. *Journal of Geophysical Research: Solid Earth*, 116(B3), 2011. doi: 10.1029/2010jb008003.

Barrie, J. V. and Greene, H. G. The Devils Mountain Fault zone: An active Cascadia upper plate zone of deformation, Pacific Northwest of North America. *Sedimentary Geology*, 364:228–241, 2018. doi: 10.1016/j.sedgeo.2017.12.018.

Bassett, D. and Watts, A. B. Gravity anomalies, crustal structure, and seismicity at subduction zones: 1. Seafloor roughness and subducting relief. *Geochemistry, Geophysics, Geosystems*, 16(5): 1508–1540, 2015. doi: 10.1002/2014gc005684.

Bellier, O., Sebrier, M., Pramumijoyo, S., Beaudouin, T., Harjono, H., Bahar, I., and Forni, O. Paleoseismicity and seismic hazard along the Great Sumatran Fault (Indonesia). *Journal of Geodynamics*, 24(1-4):169–183, 1997. doi: 10.1016/s0264-3707(96)00051-8.

Blair, J. L., McCrory, P., Oppenheimer, D., and Waldhauser, F. *A geo-referenced 3D model of the Juan de Fuca slab and associated seismicity*. US Department of the Interior, US Geological Survey, 2011. doi: 10.3133/ds633.

Blakely, R. J., Wells, R. E., Weaver, C. S., and Johnson, S. Y. Location, structure, and seismicity of the Seattle fault zone, Washington: Evidence from aeromagnetic anomalies, geologic mapping, and seismic-reflection data. *Geological Society of America Bulletin*, 114(2):169–177, 2002. doi: 10.1130/0016-7606(2002)114<0169:lsasot>2.0.co;2.

Bostock, M. G., Christensen, N. I., and Peacock, S. M. Seismicity in Cascadia. *Lithos*, 332:55–66, 2019. doi: 10.1016/j.lithos.2019.02.019.

Brocher, T. M., Wells, R. E., Lamb, A. P., and Weaver, C. S. Evidence for distributed clockwise rotation of the crust in the northwestern United States from fault geometries and focal mechanisms. *Tectonics*, 36(5):787–818, 2017. doi: 10.1002/2016tc004223.

Burgette, R. J., Weldon II, R. J., and Schmidt, D. A. Interseismic uplift rates for western Oregon and along-strike variation in locking on the Cascadia subduction zone. *Journal of Geophysical Research: Solid Earth*, 114(B1), 2009. doi: https://doi.org/10.1029/2008JB005679.

Chen, Z., Schellart, W. P., Strak, V., and Duarte, J. C. Does subduction-induced mantle flow drive backarc extension? *Earth and Planetary Science Letters*, 441:200–210, 2016. doi: 10.1016/j.epsl.2016.02.027.

Condit, C. B., Guevara, V. E., Delph, J. R., and French, M. E. Slab dehydration in warm subduction zones at depths of episodic slip and tremor. *Earth and Planetary Science Letters*, 552:116601, 2020. doi: 10.1016/j.epsl.2020.116601.

Cortés-Aranda, J., González, J., Molina, D., Astudillo-Sotomayor, L., Tassara, A., Miller, M., Álvarez Amado, F., González, R., and Bahamondes, D. Linking Upper-Plate Fault Reactivation With the Megathrust Earthquake Cycle: The Case of the Northern Chile Outer Forearc (19°S–23°S). *Tectonics*, 41(11):e2021TC006956, 2022. doi: https://doi.org/10.1029/2021TC006956.

Crouch, S. and Starfield, A. M. *Boundary Element Methods in Solid Mechanics: With Applications in Rock Mechanics and Geological Engineering*. Allen & Unwin, 1983. https://books.google.com.tr/books?id=l-6uQgAACAAJ.

Delano, J. E., Amos, C. B., Loveless, J. P., Rittenour, T. M., Sherrod, B. L., and Lynch, E. M. Influence of the megathrust earthquake cycle on upper-plate deformation in the Cascadia forearc of Washington State, USA. *Geology*, 45(11):1051–1054, 2017. doi: 10.1130/g39070.1.

DeMets, C., Gordon, R. G., and Argus, D. F. Geologically current plate motions. *Geophysical Journal International*, 181(1):1–80, 2010. doi: 10.1111/j.1365-246x.2009.04491.x.

Dimitrova, L., Wallace, L., Haines, A., and Williams, C. High-resolution view of active tectonic deformation along the Hikurangi subduction margin and the Taupo Volcanic Zone, New Zealand. *New Zealand Journal of Geology and Geophysics*, 59 (1):43–57, 2016. doi: 10.1080/00288306.2015.1127823.

Dragert, H., Hyndman, R., Rogers, G., and Wang, K. Current deformation and the width of the seismogenic zone of the northern Cascadia subduction thrust. *Journal of Geophysical Research: Solid Earth*, 99(B1):653–668, 1994. doi: 10.1029/93jb02516.

Duckworth, W. C., Amos, C. B., Schermer, E. R., Loveless, J. P., and Rittenour, T. M. Slip and strain accumulation along the Sadie Creek fault, Olympic Peninsula, Washington. *Journal of Geophysical Research: Solid Earth*, 126(3):2020JB020276, 2021. doi: 10.1029/2020jb020276.

Evans, E. L. A dense block model representing western continental United States deformation for the 2023 update to the National Seismic Hazard Model. *Seismological Society of America*, 93(6): 3024–3036, 2022. doi: 10.1785/0220220141.

Fagereng, Å., Diener, J. F., Meneghini, F., Harris, C., and Kvadsheim, A. Quartz vein formation by local dehydration embrittlement along the deep, tremorgenic subduction thrust interface. *Geology*, 46(1):67–70, 2018. doi: 10.1130/G39649.1.

Fairchild, L. H. and Cowan, D. S. Structure, petrology, and tectonic history of the Leech River complex northwest of Victoria, Vancouver Island. *Canadian Journal of Earth Sciences*, 19(9): 1817–1835, 1982. doi: 10.1139/e82-161.

Feng, L., Newman, A. V., Protti, M., Gonzalez, V., Jiang, Y., and Dixon, T. H. Active deformation near the Nicoya Peninsula, northwestern Costa Rica, between 1996 and 2010: Interseismic megathrust coupling. *Journal of Geophysical Research: Solid Earth*, 117(B6), 2012. doi: 10.1029/2012jb009230.

Finley, T., Morell, K., Leonard, L., Regalla, C., Johnston, S. T., and Zhang, W. Ongoing oroclinal bending in the Cascadia forearc and its relation to concave-outboard plate margin geometry. *Geology*, 47(2):155–158, 2019. doi: 10.1130/g45473.1.

Graham, A. Geometry, kinematics, and Quaternary activity of the brittle Leech River fault zone, southern Vancouver Island, British Columbia, Canada. Master's thesis, University of Victoria, 2018.

Greene, H. G., Barrie, J. V., and Todd, B. J. The Skipjack Island fault zone: An active transcurrent structure within the upper plate of the Cascadia subduction complex. *Sedimentary Geology*, 378: 61–79, 2018. doi: 10.1016/j.sedgeo.2018.05.005.

Groome, W. G., Thorkelson, D. J., Friedman, R. M., Mortensen, J. K., Massey, N. W. D., Marshall, D. D., and Layer, P. W. Magmatic and tectonic history of the Leech River Complex, Vancouver Island, British Columbia: Evidence for ridge-trench intersection and accretion of the Crescent Terrane. *Special Papers-Geological Society of America*, pages 327–354, 2003. doi: 10.1130/0-8137-2371-x.327.

Harrichhausen, N., Morell, K. D., Regalla, C., Bennett, S. E., Leonard, L. J., Lynch, E. M., and Nissen, E. Paleoseismic Trenching Reveals Late Quaternary Kinematics of the Leech River Fault: Implications for Forearc Strain Accumulation in Northern Cascadia. *Bulletin of the Seismological Society of America*, 111(2): 1110–1138, 2021. doi: 10.1785/0120200204.

Harrichhausen, N., Finley, T., Morell, K. D., Regalla, C., Bennett, S. E. K., Leonard, L. J., Nissen, E., McLeod, E., Lynch, E. M., Salomon, G., and Sethanant, I. Discovery of an Active Forearc Fault in an Urban Region: Holocene Rupture on the XEOLXELEK-Elk Lake Fault, Victoria, British Columbia, Canada. *Tectonics*, 42 (12), 2023. doi: https://doi.org/10.1029/2023TC008170.

Harrichhausen, N., Morell, K. D., and Regalla, C. Forearc faults

in northern Cascadia do not accommodate elastic strain driven by the megathrust seismic cycle: techreport (1.2), 2024. doi: 10.5281/zenodo.11104836.

Hasegawa, A., Yoshida, K., Asano, Y., Okada, T., Iinuma, T., and Ito, Y. Change in stress field after the 2011 great Tohoku-Oki earthquake. *Earth and Planetary Science Letters*, 355-356:231–243, 2012.

Hayward, N. and Calvert, A. J. Seismic reflection and tomographic velocity model constraints on the evolution of the Tofino forearc basin, British Columbia. *Geophysical Journal International*, 168 (2):634–646, 2007. doi: 10.1111/j.1365-246x.2006.03209.x.

Hyndman, R. D. and Wang, K. Thermal constraints on the zone of major thrust earthquake failure: The Cascadia subduction zone. *Journal of Geophysical Research: Solid Earth*, 98(B2):2039–2060, 1993. doi: 10.1029/92jb02279.

Hyndman, R. D. and Wang, K. The rupture zone of Cascadia great earthquakes from current deformation and the thermal regime. *Journal of Geophysical Research: Solid Earth*, 100(B11): 22133–22154, 1995. doi: 10.1029/95jb01970.

Hyndman, R. D., Yamano, M., and Oleskevich, D. A. The seismogenic zone of subduction thrust faults. *Island Arc*, 6(3):244–260, 1997. doi: 10.1111/j.1440-1738.1997.tb00175.x.

Johnson, S. Y., Potter, C. J., and Armentrout, J. M. Origin and evolution of the Seattle fault and Seattle basin, Washington. *Geology*, 22(1):71–74, 1994. doi: 10.1130/0091-7613(1994)022<0071:oaeots>2.3.co;2.

Johnson, S. Y., Potter, C. J., Miller, J. J., Armentrout, J. M., Finn, C., and Weaver, C. S. The southern Whidbey Island fault: an active structure in the Puget Lowland, Washington. *Geological Society of America Bulletin*, 108(3):334–354, 1996. doi: 10.1130/0016-7606(1996)108<0334:tswifa>2.3.co;2.

Johnson, S. Y., Dadisman, S. V., Childs, J. R., and Stanley, W. D. Active tectonics of the Seattle fault and central Puget Sound, Washington Implications for earthquake hazards. *Geological Society of America Bulletin*, 111(7):1042–1053, 1999. doi: 10.1130/0016-7606(1999)111<1042:atotsf>2.3.co;2.

Johnson, S. Y., Dadisman, S. V., Mosher, D. C., Blakely, R. J., and Childs, J. R. Active tectonics of the Devils Mountain fault and related structures, northern Puget Lowland and eastern Strait of Juan de Fuca region, Pacific Northwest. *U.S. Geological Survey Professional Paper*, (1643), 2001. doi: 10.3133/pp1643.

Johnson, S. Y., Blakely, R. J., Stephenson, W. J., Dadisman, S. V., and Fisher, M. A. Active shortening of the Cascadia forearc and implications for seismic hazards of the Puget Lowland. *Tectonics*, 23(1):27 pages, 2004a. doi: 10.1029/2003tc001507.

Johnson, S. Y., Nelson, A. R., Personius, S. F., Wells, R. E., Kelsey, H. M., Sherrod, B. L., Okumura, K., Koehler, R., Witter, R. C., Bradley, L.-A., et al. Evidence for late Holocene earthquakes on the Utsalady Point fault, northern Puget lowland, Washington. *Bulletin of the Seismological Society of America*, 94(6): 2299–2316, 2004b. doi: 10.1785/0120040050.

Khazaradze, G., Qamar, A., and Dragert, H. Tectonic deformation in western Washington from continuous GPS measurements. *Geophysical Research Letters*, 26(20):3153–3156, 1999. doi: 10.1029/1999gl010458.

Kimura, G. Oblique subduction and collision: Forearc tectonics of the Kuril arc. *Geology*, 14(5):404–407, 1986. doi: 10.1130/0091-7613(1986)14<404:osacft>2.0.co;2.

Leonard, L. J., Hyndman, R. D., and Mazzotti, S. Coseismic subsidence in the 1700 great Cascadia earthquake: Coastal estimates versus elastic dislocation models. *Geological Society of America Bulletin*, 116(5-6):655–670, 2004. doi: 10.1130/b25369.1.

Li, G., Liu, Y., Regalla, C., and Morell, K. D. Seismicity relocation and fault structure near the Leech River Fault Zone, southern Vancouver Island. *Journal of Geophysical Research: Solid Earth*, 123(4):2841–2855, 2018a. doi: 10.1002/2017jb015021.

Li, S., Wang, K., Wang, Y., Jiang, Y., and Dosso, S. E. Geodetically inferred locking state of the Cascadia megathrust based on a viscoelastic Earth model. *Journal of Geophysical Research: Solid Earth*, 123(9):8056–8072, 2018b. doi: 10.1029/2018jb015620.

Littel, G. F., Bostock, M. G., Schaeffer, A., and Roecker, S. Microplate Evolution in the Queen Charlotte Triple Junction & Explorer Region: New Insights From Microseismicity. *Tectonics*, 42(6):e2022TC007494, 2023. doi: https://doi.org/10.1029/2022TC007494.

Loveless, J. jploveless/tribem: tribem 1.2 (v1.2). Zenodo., 2021. doi: https://doi.org/10.5281/zenodo.5735649.

Loveless, J. P., Allmendinger, R. W., Pritchard, M. E., and González, G. Normal and reverse faulting driven by the subduction zone earthquake cycle in the northern Chilean fore arc. *Tectonics*, 29 (2), 2010. doi: 10.1029/2009tc002465.

MacLeod, N. S., Tiffin, D. L., Snavely Jr, P. D., and Currie, R. G. Geologic interpretation of magnetic and gravity anomalies in the Strait of Juan de Fuca, US–Canada. *Canadian Journal of Earth Sciences*, 14(2):223–238, 1977. doi: 10.1139/e77-024.

Malatesta, L. C., Bruhat, L., Finnegan, N. J., and Olive, J.-A. L. Colocation of the downdip end of seismic coupling and the continental shelf break. *Journal of Geophysical Research: Solid Earth*, page e2020JB019589, 2018. doi: 10.31223/osf.io/uwzbr.

Marshall, J. S., Fisher, D. M., and Gardner, T. W. Central Costa Rica deformed belt: Kinematics of diffuse faulting across the western Panama block. *Tectonics*, 19(3):468–492, 2000. doi: 10.1029/1999tc001136.

Massey, N. W. D., MacIntyre, D. G., Desjardins, P. J., and Cooney, R. T. Digital geology map of British Columbia. *BC Ministry of Energy and Mines, Geofile*, 7:2005, 2005.

Mazzotti, S., Dragert, H., Hyndman, R. D., Miller, M. M., and Henton, J. A. GPS deformation in a region of high crustal seismicity: N. Cascadia forearc. *Earth and Planetary Science Letters*, 198(1): 41–48, 2002. doi: 10.1016/s0012-821x(02)00520-4.

Mazzotti, S., Dragert, H., Henton, J., Schmidt, M., Hyndman, R., James, T., Lu, Y., and Craymer, M. Current tectonics of northern Cascadia from a decade of GPS measurements. *Journal of Geophysical Research: Solid Earth*, 108(B12), 2003. doi: 10.1029/2003jb002653.

Mazzotti, S., Leonard, L. J., Cassidy, J. F., Rogers, G. C., and Halchuk, S. Seismic hazard in western Canada from GPS strain rates versus earthquake catalog. *Journal of Geophysical Research: Solid Earth*, 116(B12), 2011. doi: 10.1029/2011jb008213.

McCaffrey, R. Slip vectors and stretching of the Sumatran fore arc. *Geology*, 19(9):881–884, 1991. doi: 10.1130/0091-7613(1991)019<0881:svasot>2.3.co;2.

McCaffrey, R. Oblique plate convergence, slip vectors, and forearc deformation. *Journal of Geophysical Research: Solid Earth*, 97 (B6):8905–8915, 1992. doi: 10.1029/92jb00483.

McCaffrey, R. Time-dependent inversion of three-component continuous GPS for steady and transient sources in northern Cascadia. *Geophysical Research Letters*, 36(7), 2009. doi: 10.1029/2008gl036784.

McCaffrey, R., Long, M. D., Goldfinger, C., Zwick, P. C., Nabelek, J. L., Johnson, C. K., and Smith, C. Rotation and plate locking at the southern Cascadia subduction zone. *Geophysical Research Letters*, 27(19):3117–3120, October 2000. doi: 10.1029/2000gl011768.

McCaffrey, R., Qamar, A. I., King, R. W., Wells, R., Khazaradze, G., Williams, C. A., Stevens, C. W., Vollick, J. J., and Zwick, P. C.

Fault locking, block rotation and crustal deformation in the Pacific Northwest. *Geophysical Journal International*, 169(3): 1315–1340, 2007. doi: 10.1111/j.1365-246x.2007.03371.x.

McCaffrey, R., King, R. W., Payne, S. J., and Lancaster, M. Active tectonics of northwestern US inferred from GPS-derived surface velocities. *Journal of Geophysical Research: Solid Earth*, 118(2): 709–723, 2013. doi: 10.1029/2012jb009473.

McCrory, P. A., Blair, J. L., Oppenheimer, D. H., and Walter, S. R. Depth to the Juan de Fuca slab beneath the Cascadia subduction margin; a 3-D model for sorting earthquakes. U.S. Geological Survey. Data Series 91, 2006. https://pubs.usgs.gov/ds/91/.

McKenzie, K. and Furlong, K. Isolating non-subduction-driven tectonic processes in Cascadia. *Geoscience Letters*, 8(1):1–12, 2021. doi: 10.1186/s40562-021-00181-z.

Meade, B. J. Algorithms for the calculation of exact displacements, strains, and stresses for triangular dislocation elements in a uniform elastic half space. *Computers & geosciences*, 33(8): 1064–1075, 2007. doi: 10.1016/j.cageo.2006.12.003.

Meade, B. J. and Loveless, J. P. Block modeling with connected fault-network geometries and a linear elastic coupling estimator in spherical coordinates. *Bulletin of the Seismological Society of America*, 99(6):3124–3139, 2009. doi: 10.1785/0120090088.

Miller, M. M., Johnson, D. J., Rubin, C. M., Dragert, H., Wang, K., Qamar, A., and Goldfinger, C. GPS-determination of along-strike variation in Cascadia margin kinematics: Implications for relative plate motion, subduction zone coupling, and permanent deformation. *Tectonics*, 20(2):161–176, 2001. doi: 10.1029/2000tc001224.

Moore, J. C. and Saffer, D. Updip limit of the seismogenic zone beneath the accretionary prism of southwest Japan: An effect of diagenetic to low-grade metamorphic processes and increasing effective stress. *Geology*, 29(2):183–186, 2001. doi: 10.1130/0091-7613(2001)029<0183:ulotsz>2.0.co;2.

Morell, K. D., Gardner, T. W., Fisher, D. M., Idleman, B. D., and Zellner, H. M. Active thrusting, landscape evolution, and late Pleistocene sector collapse of Barú Volcano above the Cocos-Nazca slab tear, southern Central America. *Bulletin*, 125(7-8): 1301–1318, 2013. doi: 10.1130/b30771.1.

Morell, K. D., Regalla, C., Leonard, L. J., Amos, C., and Levson, V. Quaternary Rupture of a Crustal Fault beneath Victoria, British Columbia, Canada. *GSA Today*, 27(3–4), 2017. doi: 10.1130/gsatg291a.1.

Morell, K. D., Regalla, C., Amos, C., Bennett, S., Leonard, L., Graham, A., Reedy, T., Levson, V., and Telka, A. Holocene surface rupture history of an active forearc fault redefines seismic hazard in southwestern British Columbia, Canada. *Geophysical Research Letters*, 45(21):11–605, 2018. doi: 10.1029/2018gl078711.

Mouslopoulou, V., Nicol, A., Begg, J., Oncken, O., and Moreno, M. Clusters of megaearthquakes on upper plate faults control the Eastern Mediterranean hazard. *Geophysical Research Letters*, 42 (23):10–282, 2015. doi: 10.1002/2015gl066371.

Nelson, A. R., Johnson, S. Y., Kelsey, H. M., Wells, R. E., Sherrod, B. L., Pezzopane, S. K., Bradley, L.-A., Koehler, R. D., and Bucknam, R. C. Late Holocene earthquakes on the Toe Jam Hill fault, Seattle fault zone, Bainbridge Island, Washington. *Geological Society of America Bulletin*, 115(11):1388–1403, 2003. doi: 10.1130/b25262.1.

Nelson, A. R., Personius, S. F., Wells, R. E., Schermer, E. R., Bradley, L.-A., Buck, J., and Reitman, N. Holocene earthquakes of Magnitude 7 during westward escape of the Olympic Mountains, Washington. *Bulletin of the Seismological Society of America*, 107 (5):2394–2415, 2017. doi: 10.1785/0120160323.

Oleskevich, D. A., Hyndman, R. D., and Wang, K. The updip and downdip limits to great subduction earthquakes: Thermal and structural models of Cascadia, south Alaska, SW Japan, and Chile. *Journal of Geophysical Research: Solid Earth*, 104(B7): 14965–14991, 1999. doi: 10.1029/1999jb900060.

Pacific Northwest Seismic Network. Seismicity Data from January 1, 1970 to April 29, 2015 [techreport], 2022. https://pnsn.org/.

Personius, S. F., Briggs, R. W., Nelson, A. R., Schermer, E. R., Maharrey, J. Z., Sherrod, B. L., Spaulding, S. A., and Bradley, L.-A. Holocene earthquakes and right-lateral slip on the left-lateral Darrington–Devils Mountain fault zone, northern Puget Sound, Washington. *Geosphere*, 10(6):1482–1500, 2014. doi: 10.1130/ges01067.1.

Pezzopane, S. K. and Weldon, R. J. Tectonic role of active faulting in central Oregon. *Tectonics*, 12(5):1140–1169, 1993. doi: 10.1029/92tc02950.

Polenz, M., Wegmann, K. W., and Schasse, H. W. *Geologic map of the Elwha and Angeles Point 7.5-minute quadrangles, Clallam County, Washington*. Washington State Division of Geology and Earth Resources, 2004.

Quigley, M., Van Dissen, R., Litchfield, N., Villamor, P., Duffy, B., Barrell, D., Furlong, K., Stahl, T., Bilderback, E., and Noble, D. Surface rupture during the 2010 Mw 7.1 Darfield (Canterbury) earthquake: Implications for fault rupture dynamics and seismic-hazard analysis. *Geology*, 40(1):55–58, 2012. doi: 10.1130/G32528.1.

Regalla, C., Fisher, D. M., Kirby, E., Oakley, D., and Taylor, S. Slip Inversion Along Inner Fore-Arc Faults, Eastern Tohoku, Japan. *Tectonics*, 36(11):2647–2668, 2017. doi: 10.1002/2017tc004766.

Rippke, J. Forearc Stresses in the Northern Cascadia Subduction Zone. Master's thesis, University of Minnesota, 2020.

Ryder, I., Rietbrock, A., Kelson, K., Bürgmann, R., Floyd, M., Socquet, A., Vigny, C., and Carrizo, D. Large extensional aftershocks in the continental forearc triggered by the 2010 Maule earthquake, Chile. *Geophysical Journal International*, 188(3): 879–890, 2012. doi: 10.1111/j.1365-246x.2011.05321.x.

Saux, J. P., Molitors Bergman, E. G., Evans, E. L., and Loveless, J. P. The Role of Slow Slip Events in the Cascadia Subduction Zone Earthquake Cycle. *Journal of Geophysical Research: Solid Earth*, 127(2):e2021JB022425, 2022. doi: https://doi.org/10.1029/2021JB022425.

Savard, G., Bostock, M. G., and Christensen, N. I. Seismicity, metamorphism, and fluid evolution across the Northern Cascadia fore arc. *Geochemistry, Geophysics, Geosystems*, 19(6): 1881–1897, 2018. doi: 10.1029/2017gc007417.

Savard, G., Bostock, M., Hutchinson, J., Kao, H., Christensen, N., and Peacock, S. The northern terminus of Cascadia subduction. *Journal of Geophysical Research: Solid Earth*, 125(6): e2019JB018453, 2020. doi: 10.1029/2019jb018453.

Schermer, E. R., Amos, C. B., Duckworth, W. C., Nelson, A. R., Angster, S., Delano, J., and Sherrod, B. L. Postglacial Mw 7.0–7.5 earthquakes on the North Olympic Fault Zone, Washington. *Bulletin of the Seismological Society of America*, 111(1):490–513, 2021. doi: 10.1785/0120200176.

Schmalzle, G. M., McCaffrey, R., and Creager, K. C. Central Cascadia subduction zone creep. *Geochemistry, Geophysics, Geosystems*, 15(4):1515–1532, 2014. doi: 10.1002/2013gc005172.

Sherrod, B. L., Blakely, R. J., Weaver, C. S., Kelsey, H. M., Barnett, E., Liberty, L., Meagher, K. L., and Pape, K. Finding concealed active faults: Extending the southern Whidbey Island fault across the Puget Lowland, Washington. *Journal of Geophysical Research: Solid Earth*, 113(B5), 2008. doi: 10.1029/2007jb005060.

Sieh, K. and Natawidjaja, D. Neotectonics of the Sumatran fault, Indonesia. *Journal of Geophysical Research: Solid Earth*, 105(B12): 28295–28326, 2000. doi: 10.1029/2000jb900120.

Sitchler, J. C., Fisher, D. M., Gardner, T. W., and Protti, M. Constraints on inner forearc deformation from balanced cross sections, Fila Costeña thrust belt, Costa Rica. *Tectonics*, 26(6), 2007. doi: 10.1029/2006tc001949.

Sternai, P., Jolivet, L., Menant, A., and Gerya, T. Driving the upper plate surface deformation by slab rollback and mantle flow. *Earth and Planetary Science Letters*, 405:110–118, 2014. doi: 10.1016/j.epsl.2014.08.023.

Stevens, V. and Avouac, J. On the relationship between strain rate and seismicity in the India-Asia collision zone: Implications for probabilistic seismic hazard. *Geophysical Journal International*, 2021. doi: 10.1093/gji/ggab098.

Thomas, A. L. Poly 3D: a three-dimensional, polygonal element, displacement discontinuity boundary element computer program with applications to fractures, faults, and cavities in the Earth's crust. Master's thesis, Stanford University, 1993.

Townend, J. and Zoback, M. D. Stress, strain, and mountain building in central Japan. *Journal of Geophysical Research: Solid Earth*, 111(B3), 2006. doi: 10.26686/wgtn.13876118.

Townend, J., Sherburn, S., Arnold, R., Boese, C., and Woods, L. Three-dimensional variations in present-day tectonic stress along the Australia–Pacific plate boundary in New Zealand. *Earth and Planetary Science Letters*, 353:47–59, 2012. doi: 10.1016/j.epsl.2012.08.003.

Van Rijsingen, E., Funiciello, F., Corbi, F., and Lallemand, S. Rough subducting seafloor reduces interseismic coupling and mega-earthquake occurrence: Insights from analogue models. *Geophysical Research Letters*, 46(6):3124–3132, 2019. doi: 10.1029/2018gl081272.

Vrolijk, P. On the mechanical role of smectite in subduction zones. *Geology*, 18(8):703–707, 1990. doi: 10.1130/0091-7613(1990)018<0703:otmros>2.3.co;2.

Wallace, L. M., Beavan, J., McCaffrey, R., and Darby, D. Subduction zone coupling and tectonic block rotations in the North Island, New Zealand. *Journal of Geophysical Research: Solid Earth*, 109 (B12), 2004. doi: 10.1029/2004jb003241.

Wang, K. Stress–strain 'paradox', plate coupling, and forearc seismicity at the Cascadia and Nankai subduction zones. *Tectonophysics*, 319(4):321–338, 2000. doi: 10.1016/s0040-1951(99)00301-7.

Wang, K. and Bilek, S. L. Invited review paper: Fault creep caused by subduction of rough seafloor relief. *Tectonophysics*, 610: 1–24, 2014. doi: 10.1016/j.tecto.2013.11.024.

Wang, K. and Tréhu, A. M. Invited review paper: Some outstanding issues in the study of great megathrust earthquakes—The Cascadia example. *Journal of Geodynamics*, 98:1–18, 2016. doi: 10.1016/j.jog.2016.03.010.

Wang, K., Wells, R., Mazzotti, S., Hyndman, R. D., and Sagiya, T. A revised dislocation model of interseismic deformation of the Cascadia subduction zone. *Journal of Geophysical Research: Solid Earth*, 108(B1), 2003. doi: 10.1029/2001jb001227.

Wang, K., Hu, Y., Bevis, M., Kendrick, E., Smalley, R., Vargas, R. B., and Lauría, E. Crustal motion in the zone of the 1960 Chile earthquake: Detangling earthquake-cycle deformation and forearc-sliver translation. *Geochemistry, Geophysics, Geosystems*, 8(10), 2007. doi: 10.1029/2007gc001721.

Wells, R. E. and McCaffrey, R. Steady rotation of the Cascade arc. *Geology*, 41(9):1027–1030, 2013. doi: 10.1130/g34514.1.

Wells, R. E., Weaver, C. S., and Blakely, R. J. Fore-arc migration in Cascadia and its neotectonic significance. *Geology*, 26(8):759–762, 1998. doi: 10.1130/0091-7613(1998)026<0759:famica>2.3.co;2.

Wells, R. E., Blakely, R. J., Wech, A. G., McCrory, P. A., and Michael, A. Cascadia subduction tremor muted by crustal faults. *Geology*, 45(6):515–518, 2017. doi: 10.1130/g38835.1.

Yoshioka, S., Wang, K., and Mazzotti, S. Interseismic locking of the plate interface in the northern Cascadia subduction zone, inferred from inversion of GPS data. *Earth and Planetary Science Letters*, 231(3-4):239–247, 2005. doi: 10.1016/j.epsl.2004.12.018.